Journal of Applied Mechanics and Technical Physics, Vol. 36, No. 6, 1995

EMERGENCE PATHS OF CRACKS ON A FREE SURFACE DURING WEDGING

V. P. Efimov, P. A. Martynyuk, and E. N. Sher

UDC 539.375

The present paper is a continuation of [1], where we mainly examined the propagation of hydraulic fracturing cracks near free surfaces. A hydraulic fracturing crack is defined on the assumption that the tangential stresses at its boundaries are zero, while the normal stresses are constant along the length. In mining, one usually employs a technique in which the working tool is a wedge. One therefore needs an adequate description of wedging.

Here the wedging is simulated by the application of a pair of localized forces whose directions are dependent on the angle of the wedge and the coefficient of friction between the wedge and the medium. The quasistatic emergence paths on a rectilinear boundary have been compared with the experimental paths derived from impacts of wedges at various angles on lucite specimens. We examined how the major parameters affected the path shape: inclination angle of nuclear crack, inclination angle of wedge axis, wedge angle, and coefficient of fraction. The algorithm used to calculate the quasistatic paths is justified for describing impact wedging, where in the experiments, the mean speed of the crack was 200-250 m/sec. We used the singular integral equation method [2-4].

We simulate the action of the wedge on the medium. By 2β we denote the wedge angle and by α_0 the deviation of the wedge axis from the vertical, which in general may not coincide with the initial nuclear crack direction. We take the area of contact between the wedge and the material as much less than the size of the crack, and then the normal and tangential stresses can be replaced by resultant localized forces **N** and **T**, which are directed respectively along the normal and along the tangent to the boundaries of the wedge. We assume that $|\mathbf{T}| = k_t|\mathbf{N}|$ ($k_t = \tan\gamma$ is the coefficient of friction between the metal and the medium). The crack in wedging thus develops under the localized forces $|\mathbf{F}| = |\mathbf{F}_1| = |\mathbf{F}_2|$, applied to the edges, which emerge on the free surface, with the direction of the forces determined by the wedge angle, coefficient of friction, and inclination angle of the wedge axis.

The [2, 3] solution method works well when the load varies smoothly along the crack. We therefore displace the points of application of the localized forces from the edges of the crack into the body, but leave their directions unchanged. We assume that the localized forces $\mathbf{F}_1$ and $\mathbf{F}_2$ are applied at the points $z_1 = (\varepsilon_1 - i\varepsilon_2)e^{i\alpha_0}$ and $z_2 = -(\varepsilon_1 + i\varepsilon_2)e^{i\alpha_0}$, where ε_1 and ε_2 are the coordinates of the points of application in the $x_1'Oy_1'$, coordinate system, which is related to the direction of the wedge axis (Fig. 1a). The localized forces are applied not to the edges of the crack but are referred to the surfaces at internal points z_1 and z_2, which is unimportant because test calculations with crack length $L \geq 4\varepsilon_1$ ($\varepsilon_1 = \varepsilon_2$) gave stress intensity coefficients at the vertex of the crack differing from standard values [2, 3] by less than 2%.

Quasistatic Formulation. Consider an isotropic elastic half-plane $y \leq 0$ containing N smooth curvilinear lines of discontinuity $L_k (k = \overline{1, N})$ beginning from the boundary (Fig. 1b). Line of discontinuity L_1 is a developing crack, while the others delimit the region in which it propagates. For example, with $N = 2$, L_2 simulates the shape of the free surface boundary. Each line of discontinuity L_k is referred to its local coordinate system $x_kO_ky_k (k = \overline{1, N})$, with (x_k^0, y_k^0) the origin of local system k in the main system and α_k the angle between the Ox and O_kx_k axes. The shape of each L_k in its local coordinate system is known and is defined by the parametric equation

$$t_k = \omega_k(\xi) = x_k(\xi) + iy_k(\xi), \quad |\xi| \leq 1, \quad t_k \in L_k.$$

Mining Institute, Siberian Division, Russian Academy of Sciences, 630091 Novosibirsk. Translated from Prikladnaya Mekhanika i Tekhnicheskaya Fizika, Vol. 36, No. 6, pp. 142-152, November-December, 1995. Original article submitted December 27, 1994.

 0021-8944/95/3606-0920$12.50

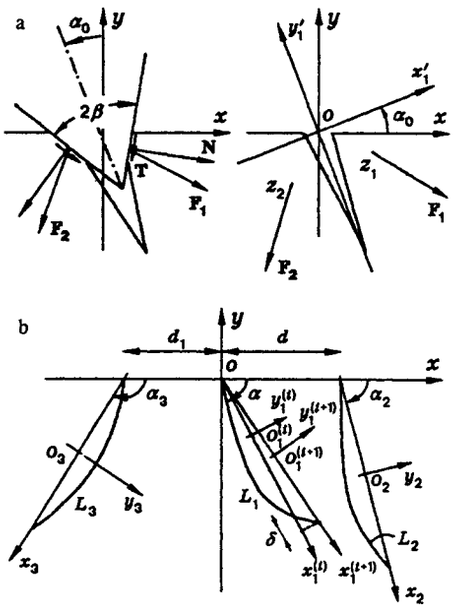

Fig. 1

We assume that the boundary of the half-plane is free from stresses. We derive the solution to the elastic problem when all the contours of the lines of discontinuity are free (the localized forces are applied at inner points of the body), which amounts to deriving N unknown functions $g_k'(\xi)$ from the following complex singular equation system [1, 3]:

$$\frac{1}{2\pi}\sum_{k=1}^{N}\int_{-1}^{1}[R_{kn}(\xi,\eta)g_k'(\xi)+S_{kn}(\xi,\eta)\overline{g_k'(\xi)}]\,d\xi = P_n(\eta)\,, \tag{1}$$

$$|\eta|\leqslant 1\,,\quad n=\overline{1,N}\,.$$

Here $g_k'(\xi) = g_k'(t_k)\omega_k'(\xi)$ and $g_k'(t_k)$ is the derivative of the displacement step:

$$\frac{d}{dt_k}[(u_k+iv_k)^+-(u_k+iv_k)^-] = \frac{i(1+æ)}{2\mu}g_k'(t_k)\quad (t_k\in L_k)\,;$$

with $æ = 3 - 4\nu$, ν Poisson's ratio (we envisage planar strain), μ the shear modulus, and

$$R_{kn}(\xi,\eta) = R_{kn}(T_k,T_n) = e^{i\alpha_k}[\zeta_{kn}(\xi,\eta)+\rho_n r_{kn}(\xi,\eta)]\,;$$

$$S_{kn}(\xi,\eta) = S_{kn}(T_k,T_n) = e^{-i\alpha_k}[\overline{\zeta_{kn}(\xi,\eta)}+\rho_n s_{kn}(\xi,\eta)]\,;$$

$$T_k = T_k(\xi) = \omega_k(\xi)e^{i\alpha_k}+z_k^0\,;\quad T_n = T_n(\eta) = \omega_n(\eta)e^{i\alpha_n}+z_n^0\,;$$

$$\zeta_{kn}(\xi,\eta) = \frac{1}{b(\xi,\eta)}-\frac{1}{\overline{a(\xi,\eta)}}-\frac{a(\xi)}{a(\xi,\eta)^2}\,;$$

$$r_{kn}(\xi,\eta) = \frac{1}{\overline{b(\xi,\eta)}}-\frac{1}{a(\xi,\eta)}+(b(\xi,\eta)-b(\eta))\frac{a(\xi)}{a(\xi,\eta)^3}\,;$$

$$s_{kn}(\xi,\eta) = b(\xi,\eta)[a(\xi,\eta)^{-2}-\overline{b(\xi,\eta)}^{-2}]\,;$$

$$a(\xi) = T_k(\xi)-\overline{T_k(\xi)}\,;\quad b(\eta) = T_n(\eta)-\overline{T_n(\eta)}\,;$$

$$a(\xi,\eta) = T_k(\xi)-\overline{T_n(\eta)}\,;\quad b(\xi,\eta) = T_k(\xi)-T_n(\eta)\,;$$

$$\rho_n = e^{-2i\alpha_n}\overline{\omega_n'(\eta)}/\omega_n'(\eta)\,;$$

$$P_n(\eta) = \frac{-|F|}{2\pi(1+\varkappa)} \sum_{s=1}^{2}(-1)^s \left\{ 2\mathrm{Re}\left[-\frac{e^{i\gamma_s}}{tz} - e^{-i\gamma_s}\frac{tz}{\overline{zt}^2} + \frac{\varkappa e^{i\gamma_s} - e^{-i\gamma_s}}{\overline{zt}} \right] + \right.$$

$$\left. + \rho_n \left[e^{-i\gamma_s}\frac{tz}{\overline{tz}^2} + (\varkappa e^{-i\gamma_s} - e^{i\gamma_s})\frac{tz}{zt^2} + e^{i\gamma_s}\left(\frac{\varkappa}{\overline{tz}} - \frac{1}{zt}\right) + \frac{e^{i\gamma_s}}{zt^3}(2(t\overline{z_s} + z_s\bar{t}) - t(\bar{t} + z_s) - \overline{z_s}(z_s + \bar{t})) \right] \right\}$$

$$(t = T_n(\eta),\ zt = z_s - \bar{t},\ tz = t - z_s,\ \gamma_1 = \alpha_0 - \beta - \gamma,\ \gamma_2 = \alpha_0 + \beta + \gamma).$$

The kernels of the singular integral equations (1) satisfy $R_{kn}(-1, \eta) = S_{kn}(-1, \eta) = 0$ $(k = \overline{1, N})$, since all the lines of discontinuity begin at the boundary of the half-plane [2-4]. The solution to (1) is sought as

$$g_k'(\xi) = \varphi_k(\xi)/\sqrt{1-\xi^2},$$

where $\varphi_k(\xi)$ is a continuous complex function in the segment $[-1, 1]$. Gauss quadrature formulas [3] give from (1) a system composed of $N(n-1)$ linear algebraic equations:

$$\sum_{k=1}^{N}\sum_{i=1}^{n}[R_{kj}(\xi_i, \eta_m)\varphi_k(\xi_i) + S_{kj}(\xi_i, \eta_m)\overline{\varphi_k(\xi_i)}] = 2nP_j(\eta_m), \tag{2}$$

$$j = \overline{1, N},\quad m = \overline{1, n-1}.$$

The value of n defines the order of approximation for the solution $\varphi_k(\xi)$, where $\xi_i (i = \overline{1, n})$ and $\eta_m (m = \overline{1, n-1})$ are the zeros of the Chebyshev polynomials $T_n(\xi) = \cos(n \arccos\xi)$ and $U_{n-1}(\eta) = \sin(n \arccos\eta)/\sqrt{1-1\eta^2}$.

To close system (2), we specify bounded displacements at the left-hand ends of the lines of section emerging on the free surface, which implies obedience to the conditions

$$\varphi_k(-1) = 0,\quad k = \overline{1, N}. \tag{3}$$

The values of $\varphi_k(\xi)$ at the ends of the lines of discontinuity at $\xi = \pm 1$ are defined by the solution of $\varphi_k(\xi_i)$ and the equations [3]

$$\varphi_k(-1) = \frac{1}{n}\sum_{i=1}^{n}(-1)^{i+n}\varphi_k(\xi_i)\,\mathrm{tg}\frac{\pi(2i-1)}{4n},$$

$$\varphi_k(1) = -\frac{1}{n}\sum_{i=1}^{n}(-1)^i\varphi_k(\xi_i)\,\mathrm{ctg}\frac{\pi(2i-1)}{4n},\quad k = \overline{1, N}. \tag{4}$$

If the solution to (2) and (3) is known, we can use integral representations for the complex potentials $\Phi(z)$, $\Psi(z)$ for a half-plane with lines of section [3, 5] and the Kolosov–Muskhelishvili formulas to determine the state of stress at each point in the region. The crack problem is that the components of the stress tensor have singularities in the region of the crack vertex. In a polar coordinate system related to the crack vertex, the following is the asymptotic distribution of the stresses in the region of the right-hand end of a curvilinear crack [2]:

$$\sigma_{\vartheta\vartheta} = \frac{k_1}{4\sqrt{2r}}\left(3\cos\frac{\vartheta}{2} + \cos\frac{3\vartheta}{2}\right) + \frac{k_2}{4\sqrt{2r}}\left(-3\sin\frac{\vartheta}{2} - 3\sin\frac{3\vartheta}{2}\right) + O(\sqrt{r}),$$

$$\sigma_{rr} = \frac{k_1}{4\sqrt{2r}}\left(5\cos\frac{\vartheta}{2} - \cos\frac{3\vartheta}{2}\right) + \frac{k_2}{4\sqrt{2r}}\left(-5\sin\frac{\vartheta}{2} + 3\sin\frac{3\vartheta}{2}\right) + O(\sqrt{r}),$$

$$\sigma_{r\vartheta} = \frac{k_1}{4\sqrt{2r}}\left(\sin\frac{\vartheta}{2} + \sin\frac{3\vartheta}{2}\right) + \frac{k_2}{4\sqrt{2r}}\left(\cos\frac{\vartheta}{2} + 3\cos\frac{3\vartheta}{2}\right) + O(\sqrt{r}).$$

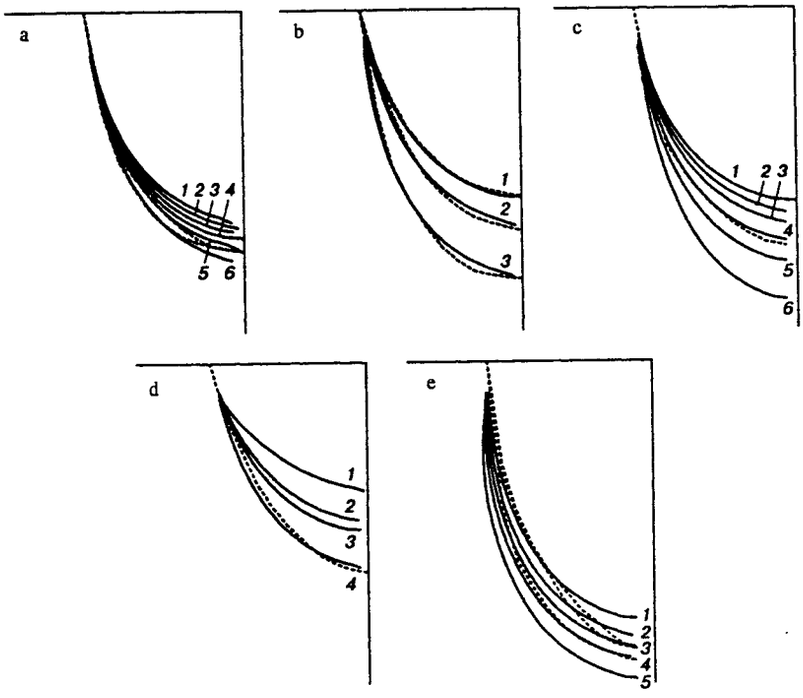

Fig. 2

The angle $\vartheta > 0$ if it is read counterclockwise from the direction of the tangent drawn to the right vertex of the crack. These expressions completely define k_1 and k_2, which are the stress intensity coefficients for the symmetrical and antisymmetrical distribution of the stresses relative to the crack line. When the crack grows in a field symmetrical with respect to it, $k_2 = 0$, and by virtue of the symmetry, the crack will propagate in its own plane. In general, when there is no local symmetry, we employ the σ_ϑ force criterion [2, 6], which has been used in numerical calculations on the experiments of [7, 8]. On that criterion, the direction of initial crack growth will coincide with the plane in which the principal part of the tensile stresses $\sigma_{\vartheta\vartheta}$ attains its maximum value. The angle defining that direction is

$$\vartheta_* = 2\operatorname{arctg}\frac{k_1 - \sqrt{k_1^2 + 8k_2^2}}{4k_2}. \tag{5}$$

For $k_1 \leq 0$, we assume that the crack cannot grow further, and the edges of it are superimposed. The critical load governing the limiting equilibrium is found from the condition that the coefficient to the singularity $(2r)^{-1/2}$ for $\sigma_{\vartheta\vartheta}$ with $\vartheta = \vartheta_*$ is equal to the critical value of the stress intensity coefficient $K_{Ic}/\sqrt{\pi}$, which is a characteristic of an elastic-brittle material:

$$\frac{1}{4}\cos^3\left(\frac{\vartheta_*}{2}\right)\left[k_1 + 3\sqrt{k_1^2 + 8k_2^2}\right] = \frac{K_{Ic}}{\sqrt{\pi}}. \tag{6}$$

The stress intensity coefficients for the first crack in the solution of (2)-(4) are given [3] by

$$k_1 - ik_2 = -\sqrt{|\omega_1'|}\,\frac{\varphi_1(1)}{\omega_1'(1)},$$

$\varphi_1(1)$ is given by (4) and k_1 and k_2 are derived only for the first crack, whose path is calculated.

Let the shape $\omega_1^{(i)}(\xi)$ of crack L_1 be known at step i in the growth, and then we solve (2) and (3) and use (5) to determine the ϑ_* indicating the direction of subsequent crack propagation. We specify the increment interval and describe the

new shape of the crack on the basis of the increase in length, i.e., we introduce the new function $\omega_1^{(i+1)}(\xi)$ ($|\xi| \leq 1$) for this crack, to get initial data for calculating the next step. In calculations on slightly inclined paths, where $|\omega_1'(\xi)| < \infty$, one can use the algorithm described in [3, 4], where at each incremental step the part of the path is approximated as a cubic parabola. The coefficients in the polynomial are derived from the conditions for smoothness of the continuation and the absence of points of inflection in the advancing part. In the present case the paths are fairly steep, and the load varies quite markedly along the crack.

Test calculations showed that one can provide fairly high accuracy with a minimum number of nodal points n if the origin in the local system is located at the center of the line of discontinuity. We use the following algorithm for constructing the path. We assume that at step i the shape of the crack $\omega_1^{(i)}(\xi)$ is described in the local coordinate system $x_1^{(i)}O_1^{(i)}y_1^{(i)}$, in which the ends of the crack at $\xi = \pm 1$ are defined by the coordinates $(\pm x_{0i}, 0)$. From the solution and the given increment δ we determine the shape of the elongated crack, which is written as $\omega_1^{(i+1)}(\xi)$ in the new local coordinate system, whose axis $O_1^{(i+1)}x_1^{(i+1)}$ passes along the chord joining the ends of the crack and the point for the origin divides the chord segment into halves. In all the calculations, the initial nuclear crack with length $2l_0$ is assumed rectilinear and usually $\varepsilon_1 = \varepsilon_2 = l_0$.

Calculated Results and Comparison with Experiment. We used lucite 100 × 100 × 10 mm. The wedging was produced by the fall of a wedge from a height of 200 mm. We used wedges having $2\beta = 30; 45; 60°$. The angle of inclination for the initial crack α was regulated by shaped supports under the specimens. The impact was not at the middle of the side of a square but a 40 mm from the right-hand edge. The wedge carried an acceleration sensor, which recorded the axial force as a function of time. The force was related to the corresponding crack length by means of thin wires, which were broken when the crack intersected them. We determined α with an error of about 5°. Also, the surface of the crack was often not orthogonal to the planes of the specimen, so the shapes of the paths on the front and rear sides differed somewhat.

The shapes of the cracks were virtually identical in static wedging and in shock wedging, when the crack moved with a mean speed of about 200-250 m/sec for identical initial angles of inclination, which leads one to hope that quasistatic calculations will apply for crack growth on impact wedging. Such calculations incorporate only the change in local stress pattern near the crack vertex caused by the elongation and curvature, while neglecting the effects from dynamic factors.

We performed calculations with $N = 3$, in which the rectilinear lines of section L_2 and L_3 were represented by the vertical boundaries of the specimen, where $d_1 = 1.5d$ (Fig. 1b); the impact was at $d = 40$ mm from the right-hand vertex of the plate. The calculated paths differed in parameters by not more than 5% from the paths with $N = 2$, where L_2 was represented by the right-hand rectilinear vertical face. The following results were obtained with $N = 2$, and the function $T_2(\xi)$ was defined by

$$T_2(\xi) = \omega_2(\xi)e^{-i\pi/2} + z_2^0 = d - il_2(\xi + 1), \quad |\xi| \leqslant 1, \quad l_2 = 2d.$$

The only adjustable parameter is the coefficient of friction. As standards we used experimental paths obtained with a wedge having $2\beta = 45°$, and $\alpha = -80°$ and $\alpha_0 = 10°$, i.e., it was assumed that the wedge axis coincided with the axis of the nuclear crack. Calculations were done with various k_t, and Fig. 2a shows the results with the indication of 2β, α, and α_0, in which the dashed lines show the standard paths and the solid lines 1-6 show the calculated paths for $k_t = 0.10; 0.15; 0.20; 0.25; 0.30; 0.40$. It is evident from Fig. 2a that the experimental paths lie between the calculated ones for $k_t = 0.3$ and 0.4. We assumed $k_t = 0.3$ in the subsequent calculations, which does not conflict with the observed value [9] and enabled one to describe all the experimental paths by means of calculated ones with an error of about 5%.

The ratio H/d characterizes the geometry of the cleaved piece (d is the distance from the mouth of the crack to the cleaving vertex, while H is the distance from that vertex to the point of emergence of the crack on the surface). The dashed and solid lines in Fig. 2b show the experimental and calculated paths for various wedge angles. Lines 1 correspond to the following parameters: $2\beta = 30°$, $\alpha = -73°$, $\alpha_0 = 17°$, $H/d = 1.17$; lines 2 correspond to $2\beta = 45°$, $\alpha = -75°$, $\alpha_0 = 15°$, $H/d = 1.40$; and lines 3 to $2\beta = 60°$, $\alpha = -82°$, $\alpha_0 = 8°$, $H/d = 1.68$. The experimental values of H/d are given.

Figure 2c shows a series of calculated paths for wedge angles $2\beta = 10; 20; 30; 45; 60; 80°$ (lines 1-6 respectively), which have been obtained for identical initial parameters $k_t = 0.3$, $\alpha = -80°$, $\alpha_0 = 10°$, while for comparison the dashed line shows the experimental path for $2\beta = 45°$. It is evident from parts *a* and *b* of Fig. 2 that increasing k_t and 2β raises H/d, since the angle between the direction of action of the localized forces and the wedge axis decreases as k_t and 2β increase, so

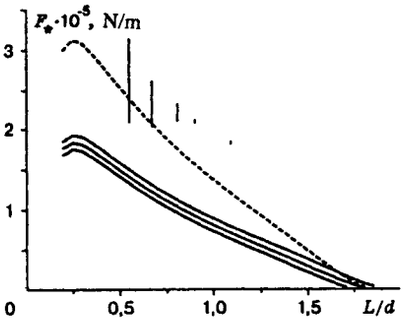

Fig. 3

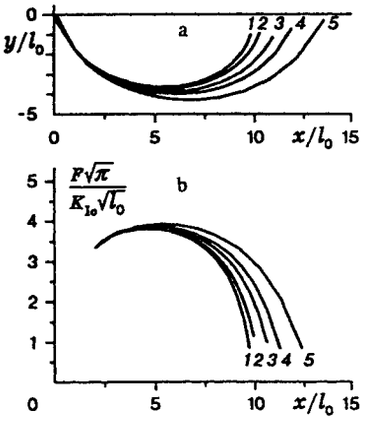

Fig. 4

the compressive components of the localized forces increase, which are directed along the crack, and which tend to straighten it out. This is confirmed by the following example.

The dashed line in Fig. 2d represents the experimental path for $2\beta = 45°$, $\alpha = -72°$, $\alpha_0 = 18°$, $H/d = 1.30$, while the solid lines are calculated paths. Path 1 was obtained with $k_t = 2\beta = 0$, an infinitely thin wedge without friction, with the localized forces directed along the normal to the axis of the nuclear crack, $H/d = 0.8$, while path 2 is for $2\beta = 0$, $k_i = 0.3$, an infinitely thin wedge with friction, with the localized forces deviating from the normal to the axis of the nuclear crack towards the vertex of the wedge by the angle $\gamma = \text{arctg}\, k_t$, $H/d = 0.98$; path 3 is for $2\beta = 45°$, $k_t = 0$, namely a wedge having $2\beta = 45°$ without friction, with the localized forces deviating in the same direction by angle β, and $H/d = 1.03$. We note that $\text{arctg}\, k_t < \beta$. Path 4 was calculated for $2\beta = 45°$ and $k_t = 0.3$, with the localized forces deviating from the normal to the axis of the wedge (at the vertex) by an angle $\beta + \gamma$, $H/d = 1.28$. This example shows that it is necessary to incorporate the wedge angle and coefficient of friction to obtain adequate results in describing wedging.

We have seen above that α is measured with a certain error in the experiments, so it is of interest to estimate how a small change in α affects the shape of the cleaved piece. On the other hand, the direction of action of the wedge may not be coaxial with the direction of the cleavage crack, i.e., the condition $\alpha_0 = \pi/2 + \alpha$ may be violated. Calculations show that these two factors have identical effects on the path shape when there are small deviations, i.e., the paths obtained with $\alpha_1 = \alpha \pm \delta\alpha$ and when the coaxiality conditions are met almost coincide with the paths calculated with inclination α for the nuclear crack and $\alpha_0^1 = \alpha_0 \pm \delta\alpha$, in which the coaxiality condition is violated by $\pm\delta\alpha$. For example, if $2\beta = 60°$, $\alpha = -77°$, $\alpha_0 = 13°$, then $H/d = 1.84$. With $\delta\alpha = \pm 3°$, we get H/d differing from the initial value by about 5%.

Figure 2e shows the effects of such deviations. Here the dashed lines show the experimental paths corresponding to $2\beta = 45°$, $\alpha = -90°$, $\alpha_0 = 0$, with $H/d = 1.80$-1.88. The calculated path 3 corresponds to these initial data. Paths 2 and 4 were calculated with the coaxiality condition obeyed for $\alpha = -88$ and $-92°$ respectively, while path I was calculated with $\alpha = -90°$, $\alpha_0 = 5°$ and path 5 with $\alpha = -85°$, $\alpha_0 = -5°$. In the last case, $\alpha = -85°$ and the angle between the direction of the cleavage crack and the direction of the wedge axis is 10°. Certain differences in the experimental paths may be due to the effects of those factors.

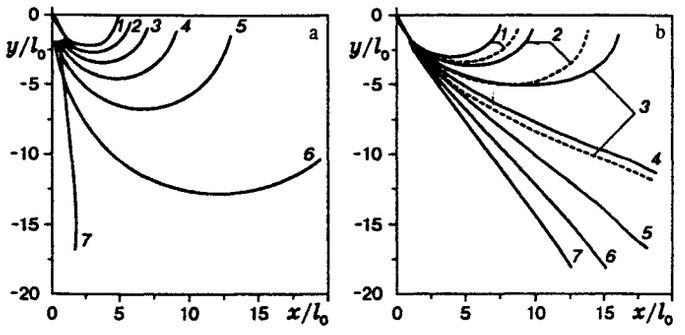

Fig. 5

From (6) we determined $k_p = K_{Ic}\sqrt{L}/F\sqrt{\pi}$, which describes the limiting equilibrium. From it we can construct the dependence of the limiting axial force $F_{\pm}$ needed to advance the crack at each step from L/d, where L is the length of the chord joining the ends of the growing crack. The force F_*, which is recorded by experiment, is defined by

$$F_* = \frac{K_{Ic}}{k_p}\sqrt{\frac{d}{\pi}}\sqrt{\frac{L}{d}}\frac{2\cos\beta[\mathrm{tg}\beta + k_t]}{\sqrt{1+k_t^2}}.$$

The calculations were performed for $k_t = 0.3$, and $K_{Ic} = 1.02\cdot10^6$ N/m$^{3/2}$, the static value for lucite.

Figure 3 shows results for a crack corresponding to $2\beta = 60°$, $\alpha = -77°$, $\alpha_0 = 13°$. The upper and lower curves correspond to change in α by $\pm3°$. The experimental F_* were determined with L/d from 0.55 to 1.10. At the first point, with $L/d = 0.55$, F_* was 3.16-2.08$\times10^5$ N/m in the experiments, while at the subsequent points, the spread is much less, and it is shown in Fig. 3 by the vertical lines. Naturally, it is difficult to expect that quasistatic calculations will give exact agreement on the variation of the limiting axial load and the experimental dependence. An approach to the experimental values can be made by incorporating the dynamics as follows. The mean crack speed in this interval is about 230 m/sec, so one can take the dynamic value for K_{Ic}, which corresponds to this velocity [9] and exceeds the static value by a factor 1.7. The dashed line in Fig. 3 corresponds to that dynamic K_{Ic}^d.

The maximum F_* increases rapidly with the wedge angle in the calculations. For example, with $k_t = 0.3$, $\alpha = -80°$, $\alpha_0 = 10°$ and wedge angle $2\beta = 10$; 30; 60; 80; 90° we get we get $F_* = (0.54; 0.92; 1.93; 3.55; 5.26)\cdot10^5$ N/m. However $2\beta = 95$-100°, the stress intensity coefficient k_1 becomes negative, i.e., a large-angle wedge cannot cleave the specimen.

It has been shown [10] that the pair of localized forces Y, directed downwards and applied to the boundary of a free half-plane at points symmetrical relative to the mouth of a free crack orthogonal to the surface will be equivalent to the action of a pair of forces $2Y/\pi$ directed horizontally and tending to compress the crack. Therefore, in wedging of a half-plane, the effective horizontal components of the localized forces decreases as the wedge angle increases and become zero when $\mathrm{tg}(\beta + \gamma) = \pi/2$. Then if $k_t = 0.3$, wedges having $2\beta > 82°$ cannot advance the crack. A similar explanation evidently applies for the present case. The calculated paths in Fig. 2 were derived for $l_0/d = 0.1$. The paths come into coincidence as this ratio decreases.

Wedging by a sharp knife, when the crack emerges on a vertical face (experimental data for lucite provided by A. F. Revuzhenko) gives $H/d = 1.27$-1.73. If we assume $2\beta = 20°$, $k_t = 0.3$, then when the initial crack deviates from the vertical by $\pm5°$, the calculated value is $H/d = 1.40$-1.73, while for $2\beta = k_t = 0$, H/d varies over the range 1.11-1.43.

Crack Emergence Path on Free Surface with Wedging. The above study concerned cracks emerging on a free vertical surface. We consider how substantially a free vertical boundary affects the results. For this purpose we consider the limiting case $d \to \infty$, i.e., $N = 1$, and we have simply a free half-plane, from the boundary of which a crack begins to grow. Here, as previously, we assume that at the initial instant a nuclear crack of length $2l_0$ is rectilinear and

$$T_1^{(1)}(\xi) = \omega_1^{(1)}(\xi)e^{i\alpha} + z_1^0 = l_0(1+\xi)e^{i\alpha}, \quad |\xi| \leqslant 1.$$

We examine how the main wedging parameters 2β, k_t, and α affect the path shape.

The shape of the path remains virtually unaltered for gently inclined paths of cracks from hydraulic fracturing emerging on free surfaces [1] as the increment step δ varies widely, whereas in our case of steep paths, it is very much dependent on

the increment step $\bar{\delta} = \delta/l_0$. Lines 1-5 in Fig. 4a show the calculated paths for $\bar{\delta} = 0.1$; 0.2; 0.4; 0.6; 1.0, corresponding to the initial parameters $2\beta = 10°$, $k_t = 0.3$, $\alpha = -60°$, $\alpha_0 = 30°$. For $\bar{\delta} \to 0$, the paths converge to the limiting one and the characteristic dimensions of the paths vary linearly with respect to $\bar{\delta}$. The basic parameters of the limiting path are less than the calculated ones for $\bar{\delta} = 0.1$ by less than 5%. Lines 1-5 in Fig. 4b show how the dimensionless limiting force $\bar{F} = \sqrt{\pi}F/K_{Ic}\sqrt{l_0}$ varies with L/l_0. There is a small initial segment of stable crack growth. The maximum values of $\bar{F}$ are only slightly dependent on $\bar{\delta}$; for example, $\bar{F} = 3.79$ for $\bar{\delta} \to 0$, while $\bar{F} = 3.94$ for $\bar{\delta} = 1.0$. This situation is one in which the shape of the emergence path for an inclined crack on a free surface is markedly dependent on the increment step and is due to the geometry, not to the choice of loading form producing the crack motion. Additional calculations have shown that this dependence on $\bar{\delta}$ occurs also for hydraulic fracturing cracks.

Figure 5a shows calculated emergence paths for inclined cracks on a free surface produced by a pair of localized forces orthogonal to the nuclear crack for the minimum value $\bar{\delta} = 0.1$. Lines 1-6 correspond to $\alpha = -60$; -65; -70; -75; -80; $-85°$. It was assumed here that $2\beta = k_t = 0$, with line 7 the path for which $\alpha = -75°$, $\alpha_0 = 0$. With that choice, the localized forces are applied at the points $z_1 = 1 - i$, $z_2 = -1 - i$, and their direction is parallel to the free surface. This model demonstrates again the stabilizing effect from the direction of action in the localized forces.

The corresponding paths for hydraulic fracturing cracks are very close to paths 1-6. Also, with $2\beta = k_t = 0$ and $\alpha_0 = \alpha + \pi/2$, all the inclined cracks emerge on the free surface. With $\alpha = -60°$, the L/l_0 dependence of $\bar{F}$ does not have a maximum, i.e., for the crack to advance further, the sufficient values of the forces are less than those corresponding to the start of motion. For $\alpha < -60°$, there are initial parts with stable crack growth, and further growth requires larger $\bar{F}$. As α approaches $-\pi/2$, the maximal $\bar{F}$ increase, and the ranges for stable crack growth are widened.

Figure 5b shows a series of calculated paths represented by solid lines 1-7 for $\alpha = -60°$, $\alpha_0 = 30°$ and the above $k_t = 0.3$, which illustrate the change in form in accordance with $2\beta = 0$; 10; 20; 30; 40; 50; 60°. For comparison, dashed lines 1-3 show the paths corresponding to $2\beta = 40°$ for $k_t = 0$; 0.1; 0.2. As k_t and 2β increase, the crack paths tend to straighten out. Figure 5b implies that for $k_t = 0.3$, only a wedge with small 2β will cleave off a piece, even for an initial crack with inclination angle $\alpha = -60°$, and the cracks tend to propagate rectilinearly as the wedge angle increases. The latter markedly distinguishes these paths from the paths of crack emergence on a free vertical surface (Fig. 2a-e) and also from the paths shown in Fig. 5a.

REFERENCES

1. T. E. Alekseeva and P. A. Martynyuk, "Crack emergence paths on a free surface," Fiz.-Tekhn. Probl. Razrabotki Polezn. Iskop., No. 2, 15-25 (1990).
2. V. V. Panasyuk, The Limiting Equilibrium of a Brittle Body Containing Cracks [in Russian], Naukova Dumka, Kiev (1968).
3. M. P. Savruk, Two-Dimensional Elasticity Problems for Bodies Containing Cracks [in Russian], Naukova Dumka, Kiev (1981).
4. M. P. Savruk, P. N. Osiv, and I. V. Prokopchuk, Numerical Analysis in Planar Problems in Cracking Theory [in Russian], Naukova Dumka, Kiev (1989).
5. P. A. Martynyuk, Crack Propagation Paths Near a Free Surface and the Boundary of a Circular Hole [in Russian]. Novosibirsk (1989), Dep. VINITI No. 2843-V89, 28.04.89.
6. V. V. Panasyuk and L. T. Berezhnitskii, "Determining limiting forces in stretching a plate containing a curved crack," Voprosy Mekhaniki Real'nogo Tverdogo Tela, No. 3 (1964).
7. S. Ya. Yarema, G. E. Ivanitskaya, A. L. Maistrenko, and A. I. Zboromirskii, "Crack growth in a solid alloy in combined deformation of types I and II," Probl. Proch., No. 8, 51-56 (1984).
8. V. V. Panasyuk, A. I. Zboromirskii, G. E. Ivanitskaya, and S. Ya. Yarema, "Applicability of the σ_ϑ criterion for forecasting a curvilinear crack path," Probl. Proch., No. 9, 3-7 (1986).
9. V. P. Efimov, "Dynamic calibration in measurements of cracking resistance in brittle materials by wedging," Fiz.-Tekhn. Probl. Razrab. Polezn. Iskop., No. 4, 89-92 (1990).
10. V. P. Efimov, P. A. Partynyuk, and E. N. Sher, "Allowance for the effects of vertical forces in wedging," Fiz.-Tekhn. Probl. Razrab. Polezn. Iskop., No. 3, 32-36 (1992).